Large-scale metasurfaces based on grayscale nanosphere lithography

Hanyu Zheng[1], You Zhou[3], Chibuzor Fabian Ugwu[2], Andrew Du[2], Ivan I. Kravchenko[4], Jason Valentine[2]*

1. Department of Electric Engineering and Computer Science, Vanderbilt University, Nashville, TN, USA
2. Department of Mechanical Engineering, Vanderbilt University, Nashville, TN, USA
3. Photonics Initiative, Advanced Science Research Center, City University of New York, New York, NY, USA
4. Center for Nanophase Materials Sciences, Oak Ridge National Laboratory, Oak Ridge, TN, USA

** Corresponding author: jason.g.valentine@vanderbilt.edu*

Abstract

Metasurfaces, based on subwavelength structuring, provide a versatile platform for wavefront manipulation in an ultra-thin form factor. The manufacturing of metasurfaces, however, generally requires fabrication techniques, such as electron-beam lithography, that are not scalable. One alternative is the use of ultra-violet steppers, but these require significant capital investment and there are challenges in handling the large mask sizes that metasurfaces demand due to the structuring density. In this paper, we proposed a novel manufacturing method based on self-assembly of nanospheres in combination with grayscale lithography. This technique enables large-scalemetasurfaces with non-periodic phase profiles while being cost-effective. As a proof of concept, we demonstrate a series of large-scale (1mm diameter) metalenses demonstrating diffraction-limited focusing as well as holograms. This approach could open new doors to cost effective and large-scale fabrication of a wide range of metasurface-based optics.

Keywords: large-scale metasurfaces, self-assembly, nanosphere lithography, grayscale lithography, metalenses

Introduction

Optical metasurfaces, based on subwavelength structuring, can provide a versatile platform for controlling the wavefront, polarization state, wave-vector, and spectral composition of light while doing so in an ultra-thin form factor[1][2][3]. This flexibility in dictating the electromagnetic response has led to numerous metasurface-based optical elements such as beam deflectors[4][5][6], holograms[7][8][9], image processors[10][11][12], bio-sensors[13][14] and metalenses[15][16][17]. The emergence of multi-element compound meta-optics offers even more flexibility in realizing complex optical assemblies[18][19][20]. However, the current conventional fabrication techniques are generally slow and result in optics that are difficult, or expensive, to manufacture at the scale of their refractive optic counterparts. Advances in affordable and scalable fabrication techniques are needed for wider scale adoption of metasurfaces and associate optical systems.

Electron-beam lithography (EBL) is the most widely used fabrication technique for visible and near-infrared metasurfaces as their feature size is typically beyond the limitation of conventional ultra-violet (UV) contact mask photolithography systems[21]. While EBL provides extremely high patterning resolution, the serial exposure process limits throughput and ultimately relegates the applicability to prototype level devices. Stepper-based lithography, on the other hand, has been proven as one of the most powerful manufacturing platforms in the semiconductor industry. These systems, through the use of focusing optics, allow for both parallel exposure and subwavelength patterning resolution. Nevertheless, the complexity of the optical system in steppers, as well as the need for high quality optical components, immersion optics, and highly accurate mechanical components results in high system cost[22]. In addition, the millions, or even billions of unit-cells comprising a metasurface results in extremely large patterning files that require algorithmic reduction based on structural symmetries[23][24]. While this reduction will work with high symmetry structures such as metalenses, it will not suffice when there is little, if any, underlying symmetry such as in holograms.

Self-assembly methods, on the other hand, provide a promising direction for large-scale device fabrication. These methods depend on a material's peculiar chemical or physical properties during bottom-up growth, for instance, block copolymer[25], DNA nanostructure[26], and nanotubes[27] can be used to realize distinctive shapes that can be utilized directly as the desired structure or as templates for further fabrication. Among these techniques, it has been demonstrated that self-assembled nanospheres can serve a means for high resolution optical lithography[28][29][30] with each sphere serving as a lens. Under illumination from a UV light source, each nanosphere will generate a photonic jet which can be used to expose an underlying photoresist. This technique can provide stepper-level spatial resolution while taking advantage of the self-assembled hexagonal lattice to locate the unit cells. Previous demonstrations of nanosphere lithography have demonstrated periodic structures such as perfect reflectors[31], absorbers[32][33] and photonic crystals[34][35]. Adjusting the substrate surface tomography allows for aperiodic structures to be realized[36] but only in relation to the position of the unit-cells while the resonators remain the same. To date, there has been no demonstration of a technique that is capable of fabricating metasurfaces with non-periodic phase profiles, such as those needed for lenses or holograms, using cost-effective self-assembly-based techniques.

Here, we demonstrate a novel manufacturing technique based on grayscale nanosphere lithography that allows for metasurfaces with arbitrary, non-periodic, phase profiles to be fabricated in a cost-effective and scalable manner. To achieve non-periodic phase control, we

combine nanosphere lithography with illumination from a spatial light modulator[37][38][39] that allows for the dose, and thus exposure size, to be controlled spatially. Furthermore, in our method we encode the resonator size into an 8-bit grayscale pattern rather than defining the geometric parameters of each individual resonator. This significantly reduces the geometric data required to write a structure leading to dramatically reduced pattern file sizes, enabling structures without an underlying symmetry. As a testbed for the technique, we fabricated a series of large-scale (diameter of 1mm) metalenses working at a wavelength of 1.7μm, demonstrating diffraction-limited focusing and above 83% relative efficiency. We also demonstrate how this technique can be used for realizing non-symmetric large-scale metasurface holograms within minimal mask sizes.

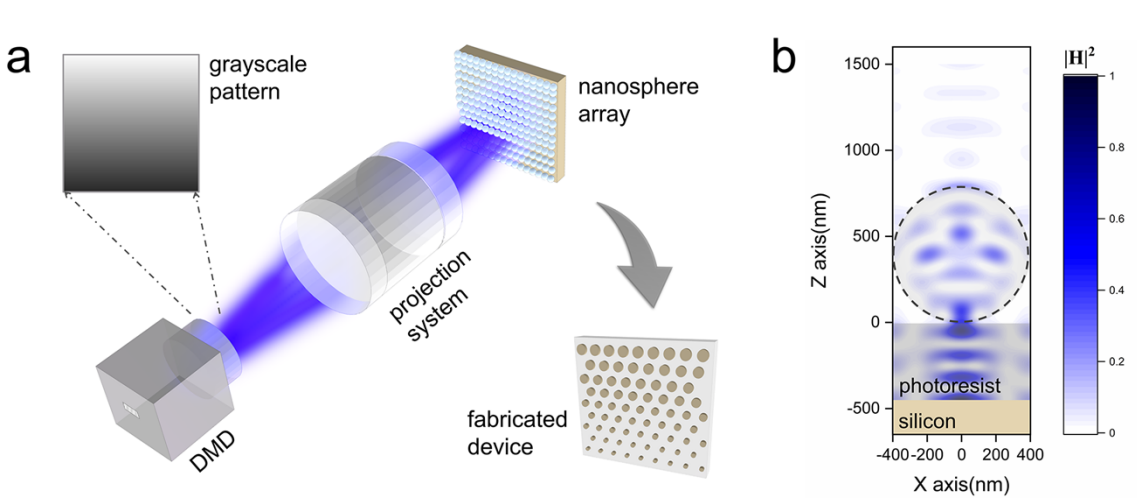

Figure 1. Self-assembly assisted large-scale metasurface fabrication platform. (a) A grayscale pattern is generated by the DMD system using a 365nm I-line UV light source which is transmitted by a projection system comprising an objective lens. The system illuminates nanospheres that have been self-assembled on the substrate and serve to focus the light. The grayscale intensity level is used to control the exposure size. for intensity modulation over substrate surface to accurately control the effective exposed area under each nanosphere. The exposed results are nonperiodic according to the exposure dosage modulation from grayscale pattern. (b) The photonic jet phenomenon, within a polystyrene nanosphere and exposure of the photoresist below. The diameter of nanosphere is 800nm in this simulation.

Results and Discussion

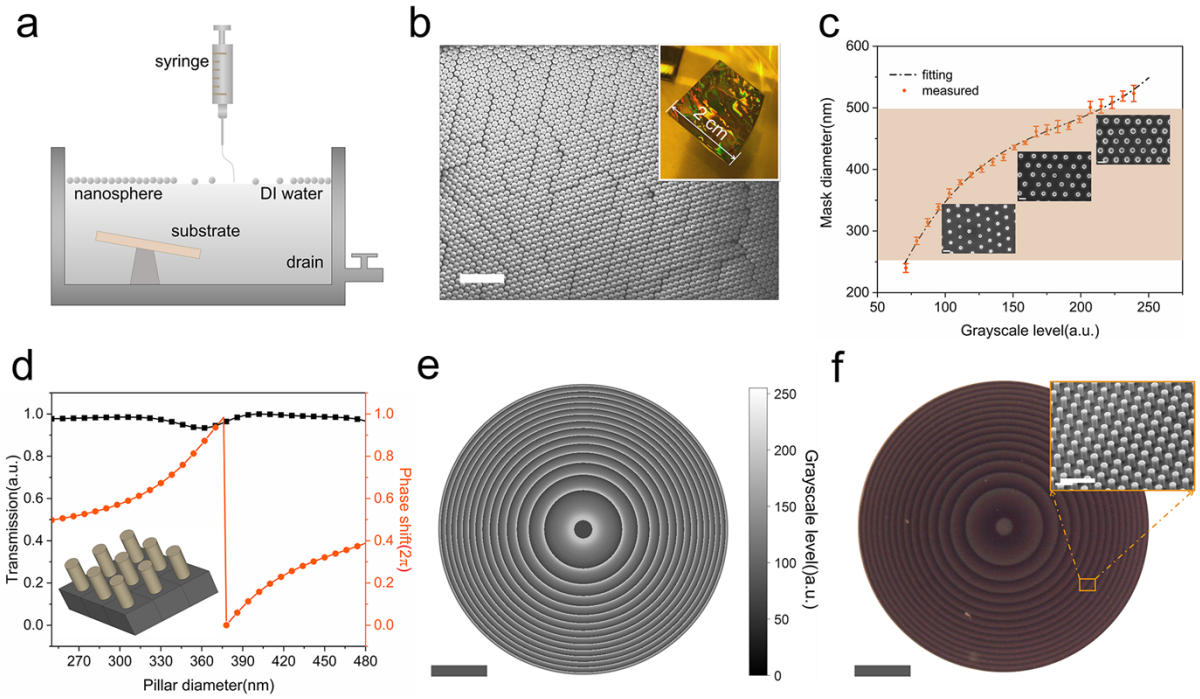

Figure 2. Fabrication results for large-scale metalenses based on grayscale lithography. (a) Schematic of air-water interface for nanosphere self-assembly. (b) SEM image of close-packed nanosphere monolayer after self-assembly. Scale bar: 5μm. Inset is an image of the entire substrate. (c) The relationship between the exposure dose, represented by grayscale level of the pattern, and the diameter of the Al_2O_3 hard mask after lift-off process. Insets are SEM images of the hard mask with different exposure doses. Scale bar: 500nm. (d) The variation of transmission and phase shift with the diameter of the silicon nanopillars. The inset depicts the simulated unit cell arranged in a hexagonal lattice. (e) The grayscale pattern corresponding to the *f*/5 metalens. Scale bar: 200μm. (f) Optical image of the fabricated *f*/5 metalens. Scale bar: 200μm. Inset is a tilted SEM image showing the silicon nanopillars. Scale bar: 2.5μm.

The fabrication approach presented here utilizes nanosphere lithography to form etch masks for patterning silicon nanopillar unit cells. The processes start with generating a monolayer of self-assembled polystyrene nanospheres. As shown in Fig. 2(a), this is accomplished by first injecting the spheres onto an air-water interface where they self-assemble into a hexagonal close-packed lattice[40][41] (see details of self-assembly process in the Methods). The wafer on which the metasurface will be fabricated, and onto which the spheres will transferred, is placed within the water bath at the start of the process. The wafers comprise a quartz handle, a silicon device layer grown via low pressure chemical vapor deposition (LPCVD), and a spin coated photoresist layer. Transfer of the self-assembled nanosphere lattice is accomplished by slowly draining the water bath. Fig. 2(b) shows an SEM image of a transferred nanosphere monolayer and the inset corresponds to an optical image where the different colors correspond to domains with different crystal orientation. The size of the nanosphere lattices is ~2cm x 2cm in the samples presented in this paper. However, past demonstrations have shown scaling to sizes of 10cm x 10cm by using larger water baths[31], indicating the potential to fabricate wafer-scale devices.

Once the nanosphere array is transferred it then serves as a lens array for exposing the photoresist beneath. We utilize a circular illumination pattern resulting in a circular exposure profile but past work has demonstrated the use of patterned masks for realizing more complicated geometries[36]. Importantly, the size of the area exposed is dictated by the illumination dosage which is a function of exposure intensity and time. To control the exposure area, and thus resonator size, we utilize a digital micro-mirror device (DMD) as a spatial light modulator. The effective exposure intensity is controlled via the duty cycle of the micro-mirrors which yields 8-bit depth and 1.6μm spatial resolution. The spatial resolution dictates the resolution at which the grayscale pattern can be modulated which is 4 nanospheres in the current system. Higher resolution could be achieved by either using either a DMD with more pixels or reducing the illumination area using higher numerical aperture (NA) projection optics. The dose-to-exposure size calibration curve was generated by depositing Al_2O_3 into the exposed photoresist patterns and measuring the diameter as a function of the grayscale level (0 to 255). The calibration curve, presented in Fig. 2c, was fitted by a quadratic polynomial curve and the mean square deviation of the diameter, which was found to be below 5%, is included as the error bars.

As a testbed for the accuracy of this fabrication method we first focus on realization of metasurface-based lenses as their performance can be quantitatively benchmarked against theoretical performance. The metalenses were designed with a hyperbolic phase profile, given by:

$$\phi(x,y) = k \times \left(f - \sqrt{x^2 + y^2 + f^2}\right) \tag{1}$$

where ϕ is the phase shift at a particular position, k is the wavenumber, and f is the focal length of designed metalens. This phase profile is converted into the grayscale pattern $G(x,y)$, where $G(x,y) = fit^{-1}\{D_\phi[\phi(x,y)]\}$ is the grayscale levels, fit^{-1} is the inverse function of the fitted curve in Fig. 2(c) and D_ϕ is the diameter of the nano-post corresponding to the required phase. D_ϕ is acquired from extracting the phase delay from full-wave simulations of hexagonal lattices of silicon nano-posts as a function of diameter, as presented in Fig. 2(d). The shaded area in Fig. 2(c) illustrates the required diameter range for achieving a 2π phase shift, based on the full-wave simulations, indicating that it is well within the grayscale patterning range. From Fig. 2(c) and Fig. 2(d) we can generate the required grayscale exposure pattern, $G(x,y)$, which is shown in Fig. 2(e) for a *f*/5 metalens with a diameter of 1mm. This pattern was used for exposure of S1805 photoresist below the self-assembled nanosphere array (see the exposure setup in Fig. S1 of the supporting materials). A 40nm Al_2O_3 hard mask was then fabricated by electronic-beam evaporation and a lift-off process. The final device was completed using reactive ion etching to form silicon pillars (see detailed fabrication process in Fig. S2 of supporting materials). An optical image of the fabricated metalens is shown in Fig.2(f) and an SEM image is in the inset.

In order to gauge the accuracy and precision of the fabrication technique, the optical properties of metalenses with *f*/5 and *f*/3 were characterized by measuring the focal spot profile at a wavelength of 1.7μm (See the detailed optical system in Methods and Fig. S3(a) of supporting materials). To evaluate the performance of each metalens, the theoretical focal spot profile was calculated based on a hyperbolic phase profile, generating diffraction-limited focal spots with full width half maxima (FWHM) of 9.06μm and 5.66μm for *f*/5 and *f*/3 lenses, respectively (Fig. 3(a)). The measured spot profiles closely match these theoretical curves, demonstrating diffraction

limited focusing. The focal spot profile along the axial axis was also recorded which was found to closely match the theoretical performance with the results presented in Fig. 3(b) and (c). These measurements demonstrate that the designed hyperbolic phase profile has been accurately realized across the metalens. The phase profile accuracy can be further verified by the imaging performance which was characterized by imaging the standard 1951 United State Air Force (USAF) test chart (Thorlabs Inc.). The image from the metalens, recorded in combination with a tube lens, is shown in Fig. 3(d) and (e) and demonstrates minimal distortion (See details of the optical system in Fig. S3(b) of the supporting materials). The increase in the numerical aperture of the *f*/3 lens results in improvement in the image quality and resolution, with the ability to resolve group 4, element 6 (line width of 17.54μm), to group 5, element 5 (line width of 9.84μm). These results indicate the capability to fabricate large-scale metalenses in a single exposure shot. In this approach, the smallest *f*/# metalens that can be fabricated can be controlled via the magnification of the projection lens in combination with the DMD resolution.

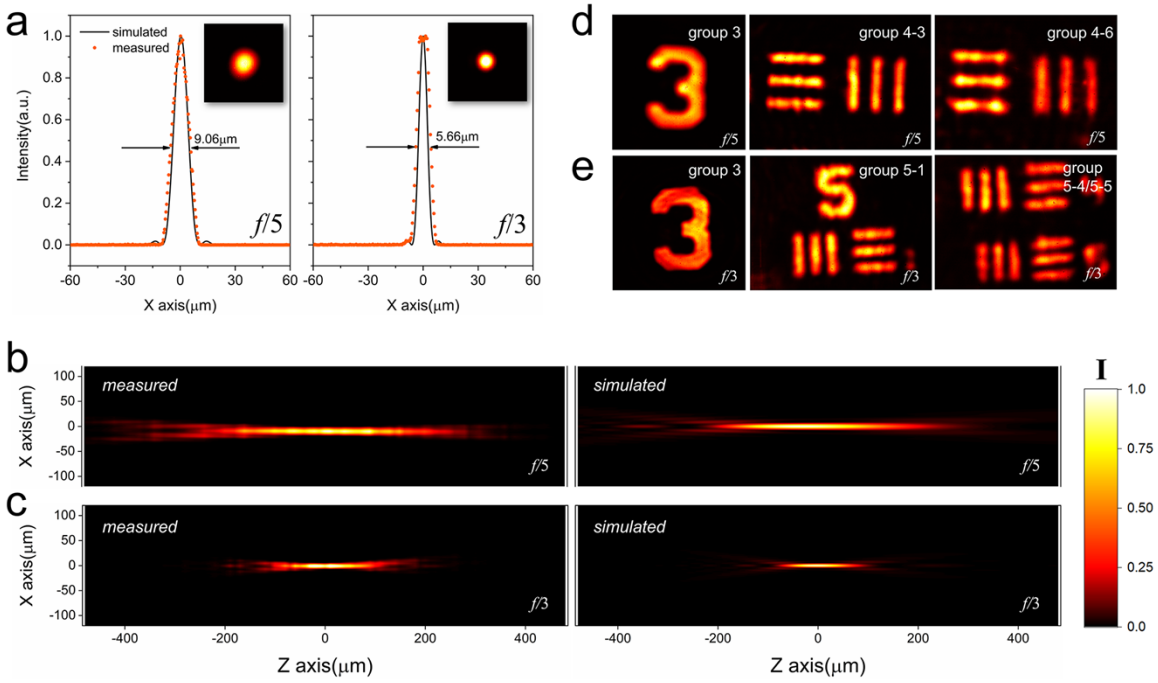

Figure 3. Experimental characterization of fabricated metalenses. (a) The measured and calculated focal spot profiles of fabricated metalenses with *f*/5(left) and *f*/3(right). Insets show the corresponding focal spot intensity distribution recorded by a NIR camera. (b) The measured (left) and experimental (right) focal spot profile along for optical axis for a metalens with *f*/5. (c) The measured (left) and simulated (right) focal spot profile along for optical axis for a metalens with *f*/3. (d) The imaging results of the USAF1951 standard test sample for the *f*/5 metalens (e) The imaging results of the USAF1951 standard test sample for the *f*/3 metalens.

The efficiency of the metalenses is the product of two factors, the relative focusing efficiency, defined as the intensity within the focal spot over all light passing through the metalens, and the transmission efficiency of the metalens. The fabricated metalenses were found to have relative focusing efficiencies of 88% and 83% for metalenses with *f*/5 and *f*/3, respectively, with a

theoretical efficiency as high as 96% for the *f*/5 metalens. The drop in experimental relative efficiency is ultimately induced by the presence of defects during self-assembly.

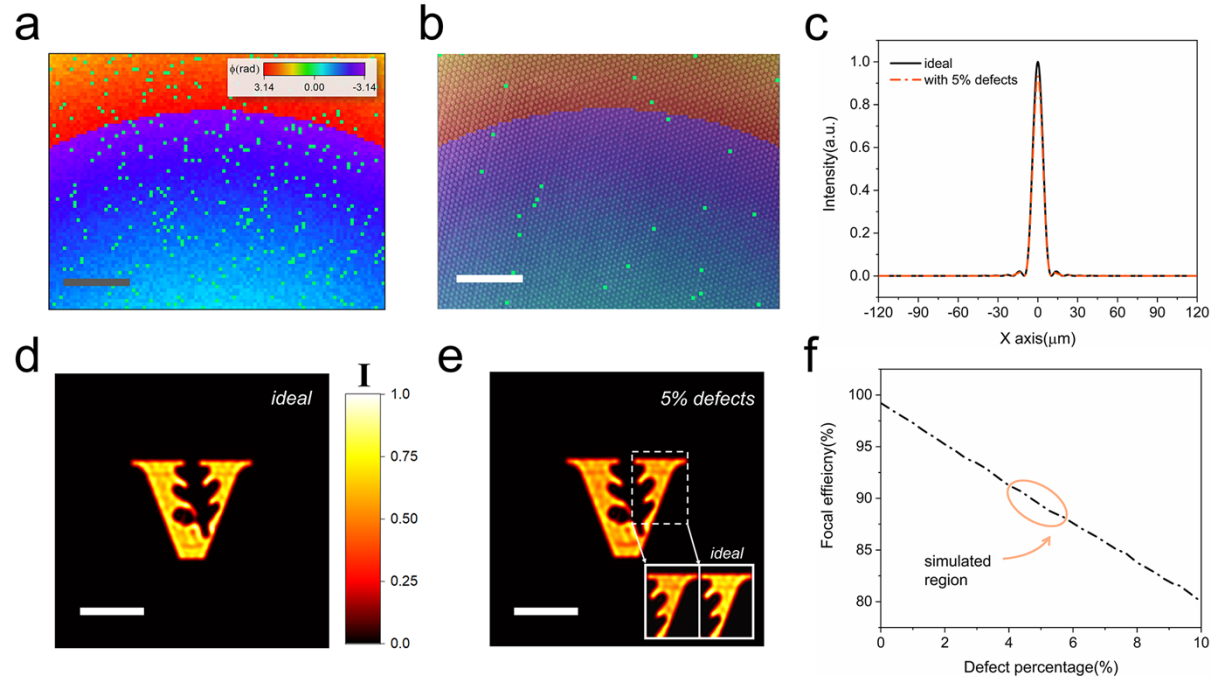

Figure 4. Roles of defects in metalens performance. (a) Phase shift profile of the designed metalens with a 5% defect density. Scale bar: 15μm. (b) SEM image of fabricated large-scale metalens. The imaged area is chosen to be close to (a) for comparison. Scale bar: 15μm. (c) The simulated focal spot profile of an ideal metalens (solid line) and one with 5% defect density (dash line), both are *f*/5. (d) Simulated imaging performance of ideal metalens with *f*/5. Scale bar: 250μm. (e) Simulated imaging performance of a metalens with the same parameters as (d) but with 5% defect density as well as a 5% phase variation. Inset: comparison of magnified region from (d) and (e). Scale bar: 250μm. (f) The simulated focusing efficiency of a metalens with *f*/5 in terms of defect density. All lenses have a working wavelength of 1.7μm. Circles indicates the defects density level in simulations.

In the case of nanosphere self-assembly, defects arise due to the size variation of polystyrene nanospheres as well as incomplete self-assembly when the lattices are being formed resulting in point defects and dislocations. To evaluate the drop of efficiency induced by these defects, we added a 5% random phase shift to each pixel to represent the standard deviation in the size of the nanospheres. Second, to represent point defects 5% of the pixels, stochastically distributed, had their phase delay set to represent air. These defect levels result in relative focusing efficiencies that were found to best match the experimental efficiencies, as described in the next section. The images of the simulated and fabricated phase profiles are shown in Fig. 4a and 4b, respectively, for comparison. The fabricated lenses have a lower point defect density with 2% of the spheres missing but also contain dislocations which have not been included in the simulated lenses.

The theoretical focal spot intensity profiles were calculated according to the Fresnel diffraction equation with the ideal phase profile taken as reference[42]. By adding a 5% defect density, as well the 5% phase shift noise into the ideal metalens phase profile, one can observe a drop of focusing efficiency to around 90% with minimal effect on the FWHM of the focal spot as shown in Fig. 4(c). The penalty in focusing efficiency is due to a transmission drop corresponding to light scattering from the defects. This scattering reduces the intensity of the image, as can be observed from the simulated images in Fig. 4(d) and (e). At the present defect density the metalens has the same resolving power with a small decline in the signal-to-noise ratio. The global relationship between focal efficiency and defect density was calculated and exhibited in Fig. 4(f). The focal efficiency can remain over 80% with a defect density of up to 10%. In the actual device, the point defect density is 2% which should result in a relative focusing efficiency of 95%. This difference between the measured (88%) and theoretical expectation most likely results from additional defects due to dislocations in the nanosphere lattice.

The measured transmission efficiency was found to be 75% for both metalenses which can be compared with a theoretical value of 97%. The drop in the experimental measurement is introduced by variations in the local period during the self-assembly process which results in the emergence of a resonance with low transmission within the nano-post structure (see the transmissive coefficient diagram in Fig. S4 of the supporting materials). This problem can be solved with the assistance of additional surfactants during the self-assembly process[43][44] or use of the Langmuir-Blodgett (LB) effect[45][46] to obtain a more uniform nanosphere array. A resonator design that is more tolerant to these types of defects would also alleviate this issue.

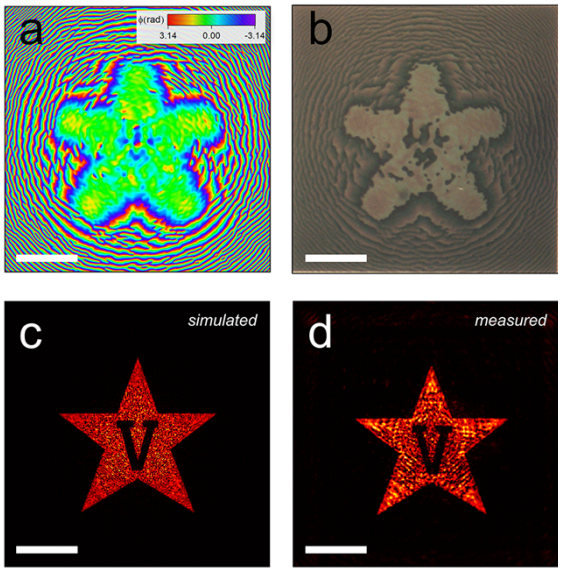

Figure 5. Demonstration of holograms. (a) Ideal phase profile of the Fresnel hologram. Scale bar: 300μm. (b) Optical image of fabricated hologram. Scale bar: 300μm. (c) Simulated hologram at the image plane. Scale bar: 300μm. (d) Measured hologram at the image plane. Scale bar: 300μm.

One technical issue associated large-scale metasurfaces is the large amount of geometrical data needed for lithography masks. While data size reduction can be realized when patterning structures with underlying symmetry, such as metalenses, there is no general technique for metasurfaces lacking such symmetry. In order to demonstrate the flexibility of our proposed method for arbitrary large-scale meta-optics fabrication, a Fresnel hologram was designed with the phase profile showed in Fig. 5(a). This hologram lacks the structural symmetry need for compression and results in a 1GB/mm^2 GDSII file based on 72 nodes being used to define each circle. Encoding the phase information into a single grayscale pattern results in a decrease in the patterning file to 0.4MB/mm^2. The hologram was designed using the Gerchberg-Saxton algorithm[47] resulting in a metasurface with only phase variations, as shown in Fig. 5(a). An optical image of the fabricated hologram is shown in Fig. 5(b)

which also demonstrates the highly aperiodic structure of the metasurface. The hologram was designed to correspond to the Vanderbilt University logo comprising a star with the letter V in the middle, the simulation of which is shown in Fig. 5 (c). This hologram was measured using a normal incident laser with the zeroth transmitted image captured by an objective lens. The resulting hologram is shown in Fig. 5(d) and demonstrates low background noise, indicating the high quality of the fabricated metasurface.

Conclusion

In summary, we have developed a novel manufacturing method for large-scale metasurfaces by combining grayscale lithography with nanosphere self-assembly. This technique allows spatially varying subwavelength nanostructures to be realized with metalenses being used as a proof of concept here, demonstrating diffraction-limited focusing performance. Although defects are unavoidable in self-assembly processes, the relative focusing efficiency of these lenses remained over 83%. Compared to conventional manufacturing platforms such as EBL and UV stepper-based lithography, our proposed method represents a cost-effective technique for large-scale device fabrication. Moreover, no reduction in mask size is necessary due to the encoding of structural variation in a grayscale pattern. The reduction in cost and patterning time associated with this technique could lead to new commercial markets where metasurface-based optics are viable.

Methods

Nanosphere self-assembly. Commercially available (EPRUI Biotech Co.) polystyrene nanosphere aqueous solution (10wt% and 3% CV) was mixed with an equal volume of methanol. 10 minutes of sonication was used to fully mix the solution before injecting onto the surface of the water using a syringe at a speed of 5μl/min. A Tygon tube with diameter of 0.55mm was connected to the syringe needle with the tube just touching the DI water surface, forming a meniscus onto which the nanospheres are deposited. Due to their hydrophobic surface, polystyrene nanospheres float on the surface of the water bath. Instead of using surfactant to accelerate the self-assembly process, which may cause nanospheres to fall from the surface, we used a flat gas nozzle to blow nitrogen onto the surface during self-assembly with a rate of 5L/min. The small perturbation on the water surface can help reorient the nanospheres[48] into a large-scale hexagonal close packaged monolayer. The nmonolayer can fill most the area of a 90mm diameter dish after around 15 minutes of the self-assembly process. The water is then drained slowly to transfer the monolayer onto the substrate which has previously been placed in the water. Due to size variation of the nanospheres, defects are unavoidable, leading to stress in the monolayer. In order to release the stress, during the transfer process the substrate was tilted by a 10° angle, which also helps to avoid formation of a multilayer structure[49].

Grayscale lithography. In order to realize dose modulation, a DMD light engine with 1920 x 1080 pixels (ZS650, Zwants Supplies, Inc.) was utilized to illuminate the grayscale pattern on the nanosphere monolayer using an I-line light source (365nm). The size of each micromirror element is 7.6μm, which was reduced to around 1.5μm by demagnification using a 5X projection lens. The diagonal length of the DMD is around 16.25mm resulting in a maximum exposure diameter of 1.6mm for a single exposure shot, after demagnification. With 8-bit color depth 256 grayscale levels can be generated which offers control over the grayscale pattern.

Numerical simulation. The complex transmission coefficient of the nano-pillars was obtained using a rigorous coupled wave analysis (RCWA) solver, reticolo[50][51]. The unit cell comprises an 850nm tall α-silicon nano-post on a quartz substrate arranged in a hexagonal lattice with a period of 800nm. The period matches the diameter of the nanospheres. The index of α-silicon (n=3.7) was acquired using ellipsometry.

Optical characterization. A custom optical imaging system was built by using a 20X objective (Mitutoyo Plan Apo, NA=0.4) for focal spot, hologram and imaging performance characterization. Illumination was provided by a supercontinuum laser (Fianium WhiteLase) passing through a monochromator (Cornerstone 130 1/8m). The light intensity was recorded by a NIR camera (Xeva-1.7-640) with background noise subtraction. Before recording the lateral focal spot profile and hologram, a standard test chart (USAF1951, R1DS1N, Thorlabs) was imaged to characterize the magnification of the optical system. To characterize the focal spot profile along the optical axis, the metalens was mounted on a translation stage with a step size of 10μm. With around 150 image slices obtained, the light intensity passing through the center of the focal spot at each image slice was rearranged along the propagating axis to form the profile image. The imaging characterization is based on the same optical system, with the USAF1951 standard test chart as the imaging target. The detailed optical system can be found in the supporting materials.

Author contributions

J.V. and H.Z developed the idea. H.Z. conducted the modelling and theoretical analysis. H.Z. fabricated the samples with assistance from Y.Z, C.F.U and A.D. I.I.K. performed the silicon growth. H.Z. performed all the experimental measurements and data analysis. H.Z. and J.V. wrote the manuscript with input from all the authors. The project was supervised by J.V.

Acknowledgements

H.Z. and J.V. acknowledge financial support by the Office of Naval Research under Grant No. N00014-18-1-2536. A.D. acknowledges support by the SyBBURE Searle Undergraduate Research Program. A portion of this research was conducted at the Center for Nanophase Materials Sciences, which is a DOE Office of Science User Facility.

Competing financial interest

The authors declare no competing financial interests.

References

[1] Lin, D.; Fan, P.; Brongersma, M. L. Dielectric gradient metasurface optical elements. *Science* **2014**, 345(6194), 298-302

[2] Yu, N.; Capasso, F.; Flat optics with designer metasurfaces. *Nature materials* **2014**, 13, 139-50

[3] Kildishev, A. V.; Boltasseva, A.; Shalaev, V. M. Planar photonics with metasurfaces. *Science* **2013**, 339(6125), 1232009

[4] Shalaev, M. I.; Sun, J.; Litchinitser, N. M. High-efficiency all-dielectric metasurfaces for ultracompact beam manipulation in transmission mode. *Nano letters* **2015**, 15(9), 6261-6266

[5] Yu, Y. F.; Zhu, A. Y.; Kuznetsov, A. I. High-transmission dielectric metasurface with 2π phase control at visible wavelengths. *Laser & Photonics Reviews* **2015**, 9(4), 412-418

[6] Yu, N.; Genevet, P.; Gaburro, Z. Light propagation with phase discontinuities: generalized laws of reflection and refraction. *Science* **2011**, 334(6054), 333-337

[7] Zheng, G.; Mühlenbernd, H.; Zhang, S. Metasurface holograms reaching 80% efficiency. *Nature nanotechnology* **2015**, 10(4), 308-312

[8] Ni, X.; Kildishev, A. V.; Shalaev, V. M. Metasurface holograms for visible light. *Nature communications*n **2013**, 4(1), 2807
[9] Huang, L.; Chen, X.; Li, J. Three-dimensional optical holography using a plasmonic metasurface. *Nature communications* **2013**, 4(1), 2808
[10] Zhou, Y.; Zheng, H.; Valentine, J. Flat optics for image differentiation. *Nature photonics* **2020**, 14(5), 316-323
[11] Cordaro, A.; Kwon, H.; Polman, A. High-index dielectric metasurfaces performing mathematical operations. *Nano letters* **2019**, 19(12), 8418-8423
[12] Zhou, J.; Qian, H.; Liu, Z. Optical edge detection based on high-efficiency dielectric metasurface. *Proceedings of the National Academy of Sciences* **2019**, 116(23), 11137-11140
[13] Leitis, A.; Tittl, A.; Altug, H. Angle-multiplexed all-dielectric metasurfaces for broadband molecular fingerprint retrieval. *Science advances* **2019**, 5(5), eaaw2871
[14] Yesilkoy, F.; Arvelo, E. R.; Altug, H. Ultrasensitive hyperspectral imaging and biodetection enabled by dielectric metasurfaces. *Nature photonics* **2019**, 13(6), 390-396
[15] Khorasaninejad, M.; Chen, W. T.; Capasso, F. Metalenses at visible wavelengths: Diffraction-limited focusing and subwavelength resolution imaging. *Science* **2016**, 352(6290), 1190-1194
[16] Arbabi, A.; Horie, Y.; Faraon, A. Subwavelength-thick lenses with high numerical apertures and large efficiency based on high-contrast transmitarrays. *Nature communications* **2015**, 6(1), 7069
[17] Zhang, L.; Ding, J.; Hu. J. Ultra-thin high-efficiency mid-infrared transmissive Huygens meta-optics. *Nature communications* **2018**, 9(1), 14181
[18] Zhou, Y.; Kravchenko, I. I.; Valentine, J. Multilayer noninteracting dielectric metasurfaces for multiwavelength metaoptics. *Nano letters* **2018**, 18(12), 7529-7537
[19] Zhou, Y.; Kravchenko, I. I.; Valentine, J. Multifunctional metaoptics based on bilayer metasurfaces. *Light: Science & Applications* **2019**, 8(1), 80
[20] Raeker, B. O.; Grbic, A. Compound metaoptics for amplitude and phase control of wave fronts. *Physical Review Letters* **2019**, 122(11), 113901
[21] Vieu, C.; Carcenac, F.; Launois, H. Electron beam lithography: resolution limits and applications. *Applied surface science* **2000**, 164(1-4), 111-117
[22] Fay, B. Advanced optical lithography development, from UV to EUV. *Microelectronic Engineering* **2002**, 61, 11-24
[23] She, A.; Zhang, S.; Capasso, F. Large area metalenses: design, characterization, and mass manufacturing. *Optics express* **2018**, 26(2), 1573-1585
[24] Park, J. S.; Zhang, S.; Capasso, F. All-glass, large metalens at visible wavelength using deep-ultraviolet projection lithography. *Nano letters* **2019**, 19(12), 8673-8682
[25] Mai, Y.; Eisenberg, A. Self-assembly of block copolymers. *Chemical Society Reviews* **2012**, 41(18), 5969-5985
[26] Yan, H.; Park, S. H.; LaBean T. H. DNA-templated self-assembly of protein arrays and highly conductive nanowires. *Science* **2003**, 301(5641), 1882-1884
[27] Reches, M.; Gazit, E. Casting metal nanowires within discrete self-assembled peptide nanotubes. *Science* **2003**, 300(5619), 625-627
[28] Haynes, C. L.; Van Duyne R. P. Nanosphere lithography: a versatile nanofabrication tool for studies of size-dependent nanoparticle optics. *Journal of Physical Chemistry B* **2001**, 105(24), 5599–5611
[29] Kosiorek, A.; Kandulski, W.; Giersig, M. Fabrication of nanoscale rings, dots, and rods by combining shadow nanosphere lithography and annealed polystyrene nanosphere masks. *Small* **2005**, 1(4), 439-444
[30] Kosiorek, A.; Kandulski, W.; Giersig, M. Shadow nanosphere lithography: simulation and experiment. *Nano letters* **2004**, 4(7), 1359-1363
[31] Moitra, P.; Slovick, B. A.; Valentine, J. Large-scale all-dielectric metamaterial perfect reflectors. *ACS photonics* **2015**, 2(6), 692-698
[32] Gwinner, M. C.; Koroknay, E.; Giessen, H. Periodic large-area metallic split-ring resonator metamaterial fabrication based on shadow nanosphere lithography. *Small* **2009**, 5(3), 400-406
[33] Walter, R.; Tittl, A.; Giessen, H. Large-area low-cost tunable plasmonic perfect absorber in the near Infrared by colloidal etching lithography. *Advanced Optical Materials* **2015**, 3(3), 398-403
[34] Han, S.; Hao, Z.; Luo, Y. Controllable two-dimensional photonic crystal patterns fabricated by nanosphere lithography. *Journal of Vacuum Science & Technology B* **2005**, 23(4), 1585-1588
[35] Oh, J. R.; Moon, J. H.; Do, Y. R. Fabrication of wafer-scale polystyrene photonic crystal multilayers via the layer-by-layer scooping transfer technique. *Journal of Materials Chemistry* **2011**, 21(37), 14167-14172

[36] Gonidec, M.; Hamedi, M. M.; Whitesides, G. M. Fabrication of nonperiodic metasurfaces by microlens projection lithography. *Nano letters* **2016**, 16(7), 4125-4132
[37] Dudley, D.; Duncan, W. M.; Slaughter, J. Emerging digital micromirror device (DMD) applications. *MOEMS display and imaging systems* **2003**, 4985, 14-25
[38] Rammohan, A.; Dwivedi, P. K.; Sharma, A. One-step maskless grayscale lithography for the fabrication of 3-dimensional structures in SU-8. *Sensors and Actuators B: Chemical* **2011**, 153(1), 125-134
[39] Sun, C.; Fang, N.; Zhang. X. Projection micro-stereolithography using digital micro-mirror dynamic mask. *Sensors and Actuators A: Physical* **2005**, 121(1), 113-120
[40] McGorty, R.; Fung, J.; Manoharan, V. N. Colloidal self-assembly at an interface. *Materials Today* **2010**, 13(6), 34-42
[41] Zhang, J.; Li, Y.; Yang, B. Colloidal self-assembly meets nanofabrication: From two-dimensional colloidal crystals to nanostructure arrays. *Advanced materials* **2010**, 22(38), 4249-4269
[42] Goodman, J. W. Introduction to Fourier optics. Roberts and Company Publishers, **2005**; pp 55-60
[43] Ye, X.; Huang, J.; Zheng, W. G. Monolayer colloidal crystals by modified air-water interface self-assembly approach. *Nanomaterials* **2017**, 7(10), 291
[44] Zhang, C.; Cvetanovic, S.; Pearce, J. M. Fabricating ordered 2-D nano-structured arrays using nanosphere lithography. *MethodsX* **2017**, 4, 229-242
[45] Parchine, M.; McGrath, J.; Pemble, M. E. Large area 2D and 3D colloidal photonic crystals fabricated by a roll-to-roll Langmuir-Blodgett method. *Langmuir* **2016**, 32(23), 5862-5869
[46] Gao, P.; He, J.; Cui, Y. Large-area nanosphere self-assembly by a micro-propulsive injection method for high throughput periodic surface nanotexturing. *Nano letters* **2015**, 15(7), 4591-4598
[47] Gerchberg, R. W. A practical algorithm for the determination of phase from image and diffraction plane pictures. *Optik* **1972**, 35, 237-246
[48] Meng, X.; Qiu, D. Gas-flow-induced reorientation to centimeter-sized two-dimensional colloidal single crystal of polystyrene particle. *Langmuir* **2014**, 30(11), 3019-3023
[49] Stavroulakis, P. I.; Christou, N.; Bagnall, D. Improved deposition of large scale ordered nanosphere monolayers via liquid surface self-assembly. *Materials Science and Engineering: B* **2009**, 165(3), 186-189
[50] Moharam, M. G.; Gaylord, T. K. Rigorous coupled-wave analysis of planar-grating diffraction. *Journal of the Optical Society of America* **1981**, 71(7), 811-818
[51] Hugonin, J. P.; Lalanne, P. Reticolo software for grating analysis. *arXiv preprint* **2021**, arXiv:2101.00901